

## Electromagnetic contributions to single-molecule sensitivity in surface-enhanced Raman scattering

Hongxing Xu,<sup>1</sup> Javier Aizpurua,<sup>2</sup> Mikael Käll,<sup>1</sup> and Peter Apell<sup>2</sup>

<sup>1</sup>*Condensed Matter Physics, Department of Applied Physics, Chalmers University of Technology, S-41296 Göteborg, Sweden*

<sup>2</sup>*Materials and Surface Theory, Department of Applied Physics, Chalmers University of Technology, S-41296 Göteborg, Sweden*

(Received 9 March 2000)

We examine whether single molecule sensitivity in surface-enhanced Raman scattering (SERS) can be explained in the framework of classical electromagnetic theory. The influence of colloid particle shape and size, composition (Ag or Au) and interparticle separation distance on the wavelength-dependent SERS enhancement factor is reported. Our calculations indicate that the maximum enhancement factor achievable through electromagnetics is of the order  $10^{11}$ . This is obtained only under special circumstances, namely at interstitial sites between particles and at locations outside sharp surface protrusions. The comparative rarity of such sites, together with the extreme spatial localization of the enhancement they provide, can qualitatively explain why only very few surface sites seem to contribute to the measured signal in single-molecule SERS experiments. Enhancement factors of the order  $10^{14} - 10^{15}$ , which have been reported in recent experiments, are likely to involve additional enhancement mechanisms such as chemisorption induced resonance Raman effects.

PACS number(s): 78.66.Bz, 73.20.Mf, 82.65.Pa, 78.30.-j

### I. INTRODUCTION

Surface-enhanced Raman scattering (SERS) is an intriguing phenomenon that can be readily observed for a range of different molecules when these are adsorbed to curved noble-metal surfaces. Despite remaining questions on the basic mechanisms involved, SERS has been developed into an important spectroscopic tool over the last two decades. Typically quoted values of the SERS enhancement factor  $M^{SERS}$ , i.e., the ratio between a measured Raman cross section in the presence and in the absence of a metal surface, range between  $10^3$  and  $10^6$  in the case of silver colloids [1]. However, recent single-molecule SERS experiments on Ag and Au colloids have indicated that a much larger enhancement factor, 10–15 orders of magnitude, may occur under special circumstances [2–7].

It is generally agreed that two fundamentally different mechanisms dominate in the SERS phenomenon—a classical electromagnetic effect and a “chemical” effect, originating in a resonance Raman enhancement of specific metal-molecule complexes [1]. The relative importance of the two effects is a matter of continuous debate, but most studies have found values for the chemical enhancement much lower than the electromagnetic contribution [8,9]. If one assumes that the two contributions can be decoupled, the integrated photon flux in a SERS experiment can be expressed as

$$\phi^{SERS} = \frac{I_I}{\hbar\omega_I} \sigma^R \sum_{i=1}^N M_i^{EM} M_i^{Ch}. \quad (1)$$

Here,  $I_I$  and  $\hbar\omega_I$  are the irradiance and energy of the incident field,  $\sigma^R$  is the temperature and wavelength-dependent Raman cross section, and  $M_i^{EM}$  and  $M_i^{Ch}$  are the electromagnetic and chemical parts of the enhancement factor, respectively, at the position of molecule  $i$ . The sum runs over all  $N$  molecules in the probe volume. Most early SERS experiments utilized large probe volumes and, consequently, most

calculations have concentrated on estimating enhancement factors averaged over positions  $i$ . In contrast, the recent single-molecule experiments were “biased” in the sense that they focused on those sites that produced such high enhancement as to render single-molecule spectroscopy possible (dubbed “hot” sites in Ref. [3]). In this context it is thus the positions  $i$  that show a *maximum* enhancement that are the most interesting. In this report we examine under what circumstances classical electromagnetic theory can produce enhancement effects of the magnitude necessary to explain single-molecule sensitivity in SERS.

Figure 1 shows transmission electron microscopy (TEM) images of a selection of colloidal Ag particles of the same type as has been found to be efficient for single-molecule SERS. It is clear that the particles are highly heterogeneous in terms of size, shape, and state of aggregation. It is thus not surprising that different particles in a particular colloid suspension exhibit different SERS characteristics, as was found in Refs. [3,6,7,10]. One question of particular interest is to what extent electromagnetics can explain “hot” isolated particles, as reported by Nie and co-workers [3], and how particle aggregation (as in Refs. [4–6,11]) affect the estimated EM enhancement. Aggregation can be induced both by the analyte itself, e.g., in the case of heme-proteins [6,12], or by high salt concentrations, as in the experiments by Kneipp *et al.* [4,5]. In the former case, the analyte can be expected to be positioned between particles in a region of extremely high-field enhancement, as will be shown below. Another important question concerns the influence of the “nanocrystallite” (i.e., nonspherical) particle morphology [3,6] (see Fig. 1) on the electromagnetic enhancement effect, in particular the effects of sharp edges. We address these issues through calculations of the electromagnetic field distributions around single Ag and Au particles and pairs of such particles. Calculations for spherical particles include retardation effects whereas the electrostatic limit is used when studying the effects of deviations from sphericity. The variation in EM enhancement with particle size, interparticle

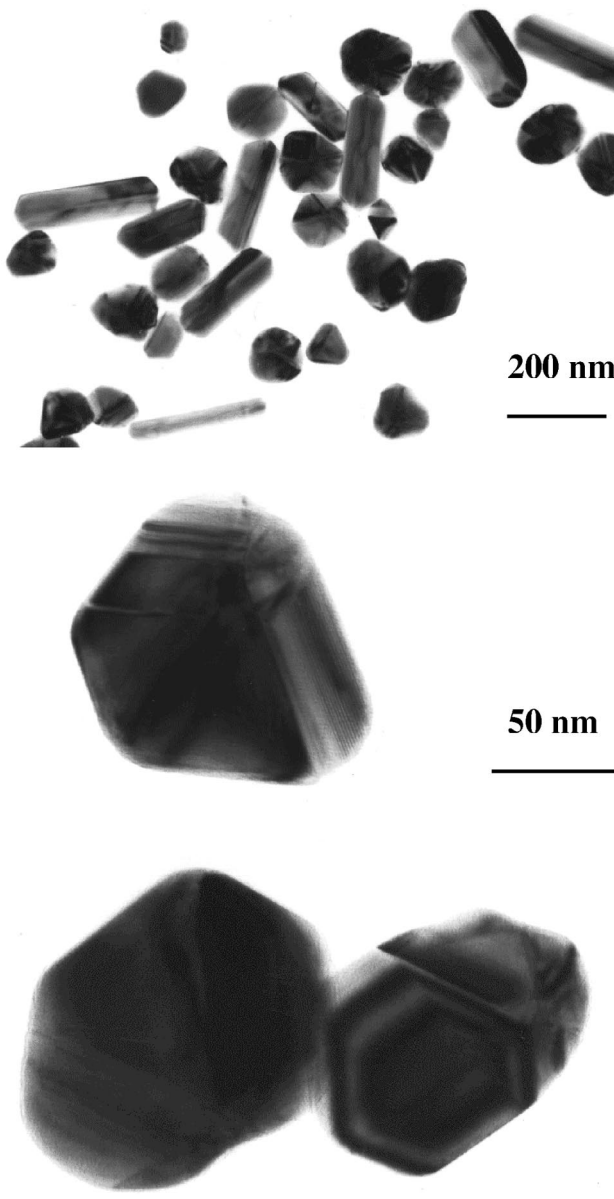


FIG. 1. Transmission electron microscope (TEM) images of Ag particles. These particles are from the same colloidal batch as used for single molecule SERS of hemoglobin, as reported in Ref. [6]. separation distance, and excitation wavelength are reported and discussed in relation to the recent SMS experiments.

## II. THEORETICAL BACKGROUND

In the electromagnetic description of SERS, the enhancement is caused by an amplification of the electric field due to the response of the material surface to the incoming wave. Depending on the material and the coupling between different surfaces, the enhancement of the local field can vary by several orders of magnitude. The EM SERS effect can be described as a consequence of the enhancement of both the incident field and the scattered field. If this enhancement is assumed to be independent of the absolute photon fluxes and polarizations involved, the EM enhancement factor can be expressed as (Stokes case) [8]:

$$M^{EM} = [E^L(\omega_I)/E^I(\omega_I)]^2 \cdot [E^L(\omega_I - \omega_v)/E^I(\omega_I - \omega_v)]^2. \quad (2)$$

Here  $E^I$  and  $E^L$  are the modulus of the incident electric field  $\mathbf{E}^I$  and the total local electric field  $\mathbf{E}^L$  in the presence of the metal, respectively. The frequency of the incident light and the vibrational frequency are denoted by  $\omega_I$  and  $\omega_v$ , respectively. Furthermore, if  $\omega_v \ll \omega_I$ , Eq. (2) can be approximated by

$$M^{EM} = [E^L(\omega_I)/E^I(\omega_I)]^4, \quad (3)$$

which shows that the local field  $E^L(\mathbf{r}, \omega)$ , taken to the fourth power, is the important quantity in the EM SERS effect. The local field can be expressed as the sum of the incident field and an induced field  $\mathbf{E}^{ind}(\mathbf{r}, \omega)$ , generated by the response of the electrodynamical environment:

$$\mathbf{E}^L(\mathbf{r}, \omega) = \mathbf{E}^I(\mathbf{r}, \omega) + \mathbf{E}^{ind}(\mathbf{r}, \omega). \quad (4)$$

A number of different techniques have been applied in the calculation of the induced field in various configurations. Here we start by modeling the metal particles as perfect spheres, which can be treated analytically in the framework of a fully retarded formalism. The local field can be obtained from the self-consistent integral equation [13]:

$$\mathbf{E}^{ind}(\mathbf{r}, \omega) = \int G(\mathbf{r}, \mathbf{r}') \nu(\omega, \mathbf{r}') \mathbf{E}^L(\mathbf{r}', \omega) d\mathbf{r}', \quad (5)$$

where  $G$  is a tensor Green function relating points  $\mathbf{r}$  and  $\mathbf{r}'$ , and

$$\nu(\omega, \mathbf{r}') = (\omega/c)^2 [\varepsilon_2 - \varepsilon(\mathbf{r}', \omega)] \quad (6)$$

with  $\varepsilon(\mathbf{r}', \omega)$  being the dielectric function at the point  $\mathbf{r}'$ , which is denoted  $\varepsilon_1$  for the metal particle and  $\varepsilon_2$  for the surrounding medium. For a single metallic sphere, the local field can be calculated following standard methods of electrodynamics [14]. In the case of two neighboring metal spheres we have adopted the technique developed by Inoue and Ohtaka [13], which is based on the multipole expansion method of Bruning and Lo [15] and the coordinate transformation methods of Stein [16] and Cruzan [17].

As we deviate from the spherical shape, in order to simulate the observed nanocrystallite particle morphology, a more suitable method is needed. Here we employ the boundary charge method (BCM) in a nonretarded scheme to deal with such morphologies [18,19]. In the framework of the BCM, the induced field  $\mathbf{E}^{ind}(\mathbf{r}, \omega)$  is obtained from the surface charge density distribution  $\sigma(\mathbf{s}', \omega)$  over the interfaces through:

$$\mathbf{E}^{ind}(\mathbf{r}, \omega) = - \int \frac{(\mathbf{r} - \mathbf{s}')}{|\mathbf{r} - \mathbf{s}'|^3} \sigma(\mathbf{s}', \omega) d\mathbf{s}', \quad (7)$$

where the integral extends over all boundaries separating two different dielectric functions. The surface charge density at the particle boundaries is obtained by numerically solving the following self-consistent equation:

$$\Lambda \sigma(\mathbf{s}, \omega) = \mathbf{n}_s \cdot \mathbf{E}^I(\mathbf{s}, \omega) - \int \frac{\mathbf{n}_s \cdot (\mathbf{s} - \mathbf{s}')}{|\mathbf{s} - \mathbf{s}'|^3} \sigma(\mathbf{s}', \omega) d\mathbf{s}', \quad (8)$$

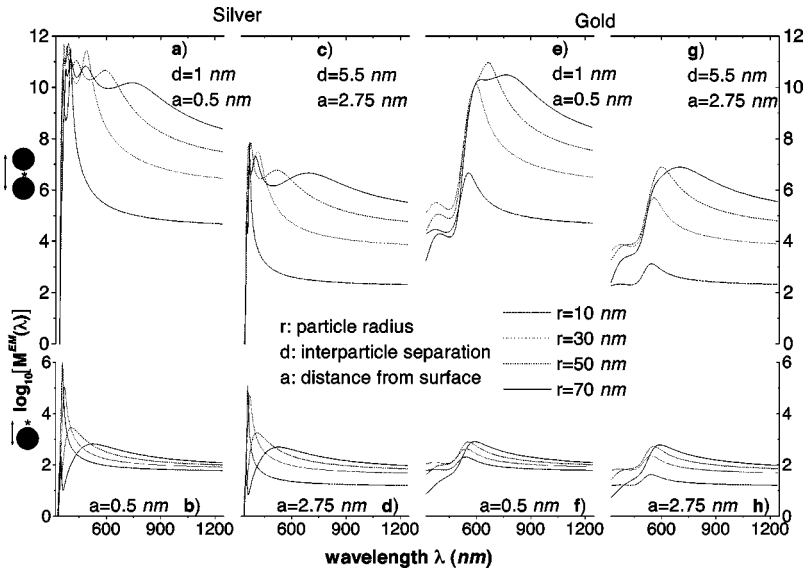


FIG. 2. Upper row shows the EM-enhancement factor  $M^{EM}$  versus wavelength at the midpoint between two equal radius spherical particles, composed of silver (a,c) and gold (e,g), separated by a gap of  $d=1$  nm (a,e) and  $d=5.5$  nm (c,g) for various radii  $r$ . When one particle is removed the EM-enhancement factor decreases dramatically, as illustrated by the data for single particles shown in the lower row (b,f,h). Calculations, based on Eqs. (3)–(6), have been performed for the optimum polarization configuration, i.e. for a polarization parallel to the dimer axis, and for the case when the surrounding medium is vacuum ( $\epsilon_2=1$ ). The dielectric constant of the particles ( $\epsilon_1$ ) is based on the experimental data of Johnson and Christy [22]. Note the logarithmic scale for  $M^{EM}$ .

where the vector positions  $s$  and  $s'$  refer to interface points,  $\mathbf{n}_s$  is the unit vector normal to the interface at point  $s$ , and  $\mathbf{E}^I(s, \omega)$  is the  $\omega$  component of the incident field acting at  $s$ :

$$\Lambda = 2\pi \frac{\epsilon_2(\omega) + \epsilon_1(\omega)}{\epsilon_2(\omega) - \epsilon_1(\omega)} \quad (9)$$

depends on the two dielectric functions  $\epsilon_1$  and  $\epsilon_2$  characterizing each medium surrounding the interface. Assuming rotational invariance, Eq. (8) can be properly projected by means of an expansion in the azimuthal angle  $\varphi$ , which facilitates the numerical procedure by describing the interfaces by means of a one-parameter curve. Details of the procedure can be found elsewhere [19]. This equation is equivalent to Poisson's equation, and a reasonable approximation to the full electromagnetic treatment when the particle length scale is small compared to the incoming wavelength. As the size of the particles becomes larger one should include retardation, as we do in the case of spherical particles. However, for the aim of investigating the qualitative effects of deviations from perfect sphericity, the BCM method constitutes a convenient and useful tool as we will now demonstrate.

### III. RESULTS AND DISCUSSION

#### A. Dependence on wavelength, size, and interparticle separation distance

We begin by analyzing the variation of  $M^{EM}$  with incident wavelength for different particle sizes. The effects of aggregation are investigated through the limiting case of a dimer configuration. As discussed in Sec. I, we evaluate  $M^{EM}$  at positions, and for polarization geometries, that produce maximum enhancement. In the dimer case this corresponds to the interstitial position, between the particles, and a polarization parallel to the dimer axis [20,21]. Figure 2 shows  $M^{EM}$  versus wavelength at the midpoint between two spheres with a surface separation of  $d=1$  nm and  $d=5.5$  nm, and for the equivalent positions outside a single sphere. The particular  $d$  values of 1 and 5.5 nm roughly correspond to the size of a small aromatic molecule, such as the dye molecule R6G, and a hemoglobin molecule, respec-

tively. The distinct peaks at certain wavelengths in Fig. 2 are due to surface plasmon resonances characteristic of each specific configuration. Because of the presence of these peaks, the enhancement factor is very sensitive to the wavelength of the incident and scattered radiation. As an example,  $M^{EM}$  changes more than 6 orders of magnitude for the case of a 10 nm particle dimer when the wavelength is shifted from the strongest resonance (at around 400 nm) to the NIR region, as can be seen in Fig. 2(a). It is also clear that the small decrease in  $d$  from 5.5 to 1 nm yields a dramatic increase in  $M^{EM}$ , and that the dimer configuration always leads to a higher enhancement than a single particle, irrespective of wavelength. This result is, of course, expected in view of the original works of Inoue and Ohtaka [13], Gersten and Nitzan [23] and others. The importance of interparticle coupling has also been emphasized in more recent reports. García-Vidal and Pendry [24], for example, modeled rough surfaces in a retarded treatment, and found local enhancement factors up to  $10^8$  in semicylindrical crevices.

In the case of single isolated particles, the surface plasmon resonances are associated with oscillations of the surface charge density of different order ( $l, m$ ), where  $l = 1, 2, 3, \dots$  (Mie frequencies [25]) corresponds to well established patterns of oscillation (dipolar, quadrupolar,  $\dots$ ). As the size of the particle increases, the peaks are shifted up in wavelength, according to the dispersion relation for radiative modes in a sphere [26]. The general increase in the polarizability with particle size leads to a modest increase of  $M^{EM}$  with radius  $r$  for large wavelengths. In the case of a dimer, the single-particle modes are replaced by coupled resonances. The strong increase in  $M^{EM}$  for the dimer case compared with the singlet is due to two influencing factors: On the one hand, the coupling of singlet resonances in the dimer situation, and on the other hand, a general background enhancement derived from the presence of the two interfaces which localize the potential drop to a confined region. At the interstitial position, and for the parallel polarization configuration, the dominant collective resonances can be interpreted as antisymmetric combinations of the original ( $l, m=0$ ) single-sphere Mie resonances [20]. With decreasing interparticle distance and increasing particle size, these collective

resonances are shifted towards longer wavelengths since the dispersion is controlled by purely geometrical effects through the parameter  $r/(2r+d)$  [20]. It is these geometrical effects, together with nearly equal electron densities, which explain the close similarity between Ag and Au in the “free-electron” region above  $\lambda \approx 600$  nm for all sizes and configurations.

From the calculations presented above, it appears unlikely that a total SERS enhancement as large as  $10^{14}$  can be induced by electromagnetics alone. In the case of nearly touching Ag spheres,  $M$  approaches  $10^{12}$  at around 400 nm, but decays by one or two orders-of-magnitude towards the visible region probed by recent experiments. An enhancement factor of around  $10^{10}$  is in general agreement with our recent experiments on hemoglobin [6], although one should note that if the separation distance is increased to 5.5 nm, in order to actually accommodate the Hb molecule, the enhancement drops by about three orders of magnitude. There is thus clearly room for additional modes of enhancement in single-molecule SERS, in particular intrinsic or chemisorption induced resonant Raman effects (RR) as well as the local response of the molecule itself [27]. In fact, even a modest RR enhancement of around three orders of magnitude will bridge the gap between experiments and electromagnetic theory in the case of the dimer configurations. On the other hand, electromagnetics applied to single spherical particles can obviously not explain single molecule sensitivity in SERS, even if RR effects are invoked. Thus, EM induced single molecule–single particle SERS has to involve morphological features that are able to concentrate the EM field in a similar way as in the dimer case, as discussed in Sec. III C.

### B. “Hot” sites

One of the most interesting questions raised by the recent single-molecule SERS experiments concerns the mechanism behind the localization of the enhancement effect into hot sites. In this paragraph we investigate the spatial extent of regions with high field enhancement with this question in mind. Figure 3 shows the enhancement factor  $M^{EM}$  in a plane through the particle centers, and normal to the propagation direction of the incident field, for a few different particle configurations and shapes. The polygonal particles show rotational symmetry around the vertical direction and have an edge angle of  $144^\circ$ , of the same magnitude as one may expect in fcc crystalites with (1,1,1) and (1,0,0) facets. The calculation has been performed for the same polarization direction and the same interparticle separation as in Fig. 2. Figure 3 clearly shows the high degree of field localization in the region between particles in a dimer. This contrasts with the case of single particles, where the enhancement is distributed widely around the two particle poles in the direction of the polarization of the incoming light. The introduction of edges, in the model with rotationally symmetric polygons, does not dramatically modify either the magnitude of the enhancement, or its spatial distribution, indicating the usefulness of the spherical approximation in the case of crystallites with large angled edges.

The images in Fig. 3 were calculated for a wavelength of 514.5 nm, commonly used in Raman spectroscopy, and for the case of Ag particles. However, the spatial distribution of

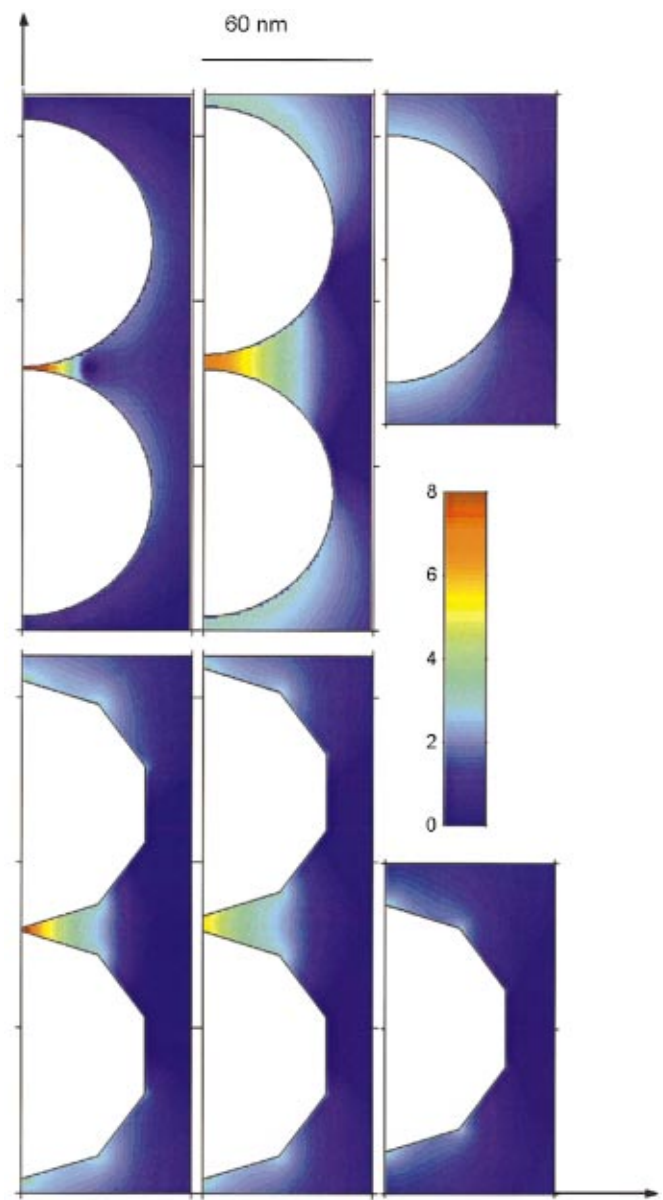


FIG. 3. (Color) EM-enhancement factor  $M^{EM}$  at a cross section through six different silver particle configurations. The wavelength of the incident field is  $\lambda = 514.5$  nm with vertical polarization. The left-hand column illustrates the EM enhancement for dimer configurations of two spheres (top) and two polygons (bottom) with a separation of 1 nm. The middle column shows the same situation, but with a separation distance of 5.5 nm. The right-hand column shows the case of an isolated single particle. All particles share a common largest dimension of 90 nm. Note that the color scale from dark blue to dark red is logarithmic, covering the interval  $10^0 < M^{EM} < 10^8$ . Regions with enhancement outside this interval are shown in dark blue and dark red, respectively.

the EM enhancement is essentially identical for all wavelengths within the visible-NIR region and also for the case of gold particles, though the absolute magnitude is different, see Fig. 2. In Fig. 4, we show the variation of  $M^{EM}$  as a function of the distance from the origin, located at the midpoint between the two particles. We examine the variation of enhancement both along the parallel (a) and perpendicular (b) direction to the dimer axis. There is a negligible variation along the dimer axis and a rapid decay of  $M^{EM}$  in the per-

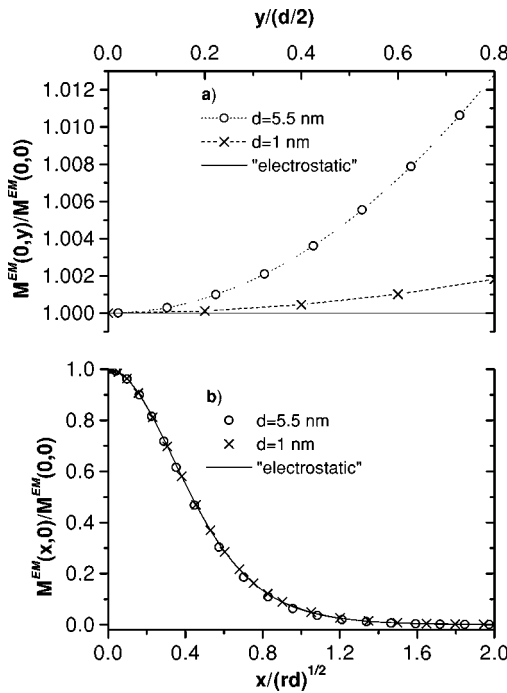


FIG. 4. Variation in the EM-enhancement factor  $M^{EM}$  within the cavity between two neighboring particles along the two principal directions parallel to the dimer axis (a) and perpendicular to the dimer axis (b). The  $M^{EM}$  factor has been normalized by the value at the midpoint. Circles and crosses represent exact calculations for separation distances of  $d=5.5$  nm and  $d=1$  nm, respectively. The solid lines represent a simple electrostatic model for two perfectly conducting cylinders in a uniform static field.

pendicular direction. These features can be well understood by a straight comparison with the electrostatic case of two cylindrical wires of diameter  $D=2r$  separated by a distance  $d$ . In this case, the perpendicular decay in the  $x$  direction can be simply described by  $M^{EM}=[b/(b-q)]^4$ , where  $b=1+d/D$  and  $q=\sqrt{1-(x/r)^2}$ . This approximation shows the main features of the localization of the high electromagnetic enhancement. The important point in Fig. 4, however, is that the region of high EM enhancements have a limited spatial extent in all directions. From the electrostatic model we find that the volume of high enhancement scales as  $d(\sqrt{rd})^2$  which is fulfilled extraordinarily well in the case of the full calculation as checked in the figure. Hence, in systems of aggregated particles, where interparticle separation can be expected to be small, we predict a very localized region of ultrahigh EM enhancement in agreement with the majority of recent single-molecule SERS reports [3–7].

### C. Effects of surface protrusions and crevices in single particles

In the previous sections we showed that spherical or “nanocrystal” shaped *single* particles cannot induce an EM enhancement of the magnitude required to explain single-molecule SERS. We now investigate whether this can be achieved in situations where substantial morphological changes in the shape of the single particle exist. Two different models are employed: a dropletlike shape, as shown in the inset of Fig. 5, and a model with two intergrown spherical particles, as shown in the inset of Fig. 6. Calculations are

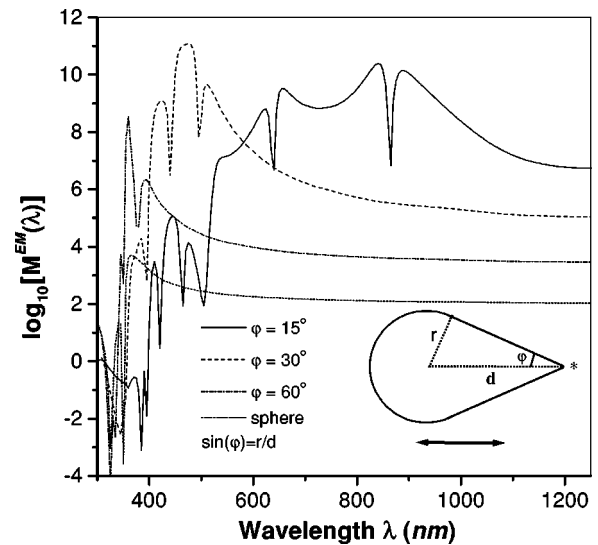


FIG. 5. EM-enhancement factor for a rotationally symmetric silver droplet as a function of the angle defining the opening edge  $\phi$ . The field is polarized parallel to the axis of the droplet and the evaluation position (star) is located 0.5 nm outside the tip. As the droplet becomes sharper the enhancement increases several orders of magnitude.

performed for Ag using the BCM [19], i.e., retardation effects are not included.

The radius  $r$  of the droplet-shaped particle is fixed to 45 nm and the semiangle of the protrusion  $\phi$  is varied from 90° (sphere with no protrusion) down to 15° (sharp protusion). The EM-enhancement factor is evaluated 0.5 nm outside the droplet protrusion in the direction of the symmetry axis for the case when the electric field is polarized in the same direction. As can be seen from Fig. 5, the presence of the protrusion increases the enhancement factor dramatically, up to the order  $10^{11}$  for  $\phi=30^\circ$ , when compared to the case of a perfectly spherical particle. This increase in  $M^{EM}$  is accompanied by an equally dramatic redshift of the resonance

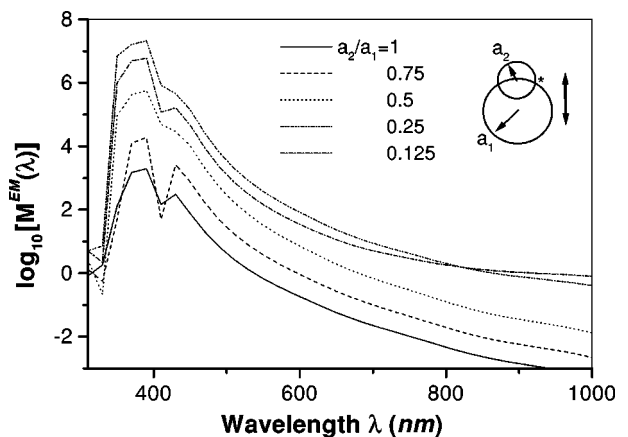


FIG. 6. EM-enhancement factor for a configuration formed by two interpenetrating spheres of radius  $a_1=45$  nm and  $a_2$ , as a function of  $a_2$ . The enhancement factor is evaluated at 0.5 nm outside the junction between the two particles for a polarization parallel to symmetry axis. The enhancement factor is found to be highly sensitive to the characteristics of the “cavity” formed by the particle intergrowth.

wavelengths. These effects are due to the increasing confinement of the surface charge density at the sharp edge, which gives rise to a stronger coupling shifting the modes positions. The resonance's dispersion with angle in Fig. 5 is similar to that in other edgelike structures, as reported by, e.g., Davis [28], and essentially follows the behavior for a solid cone. We should note that results qualitatively similar to those in Fig. 5 were obtained by Wang and Kerker [29] and Gersten and Nitzan [30] for the cases of prolate spheroids and spheroidal protrusions on a conducting plane, respectively, for various spheroid aspect ratios.

The second model consists of two interpenetrating spheres, where one of the spheres of radius  $a_1 = 45$  nm is hosting a second sphere of radius  $a_2$  simulating an intergrowth between colloidal particles. The origin of the second sphere is located at the surface of the first one. This type of structure could well be formed during colloid preparation from a seed consisting of two aggregated particles of different size. For a polarization parallel to the symmetry axis of the system, the enhancement is found to be highest in the region where the two particle surfaces meet. Outside this "crevice,"  $M^{EM}$  is not dramatically different from the case of a single spherical particle. The enhancement factor is thus analyzed as a function of the ratio  $a_1/a_2$  at 0.5 nm outside the junction between the two spherical surfaces, a location which also should be a favorable site for molecular adsorption. As is clearly shown in Fig. 6, the enhancement factor depends critically on the parameter  $a_1/a_2$ . As this ratio decreases,  $M^{EM}$  first increases rapidly, due to the change of orientation of the junction with respect to the polarized field, then passes a maximum at around  $a_1/a_2 = 0.25$ , after which a gradual decrease towards the single sphere limit at  $a_1 = 0$  occurs according to the tendency of the junction to progressively open and eventually make the aggregate disappear. The maximum EM enhancement obtained in the interpenetrating spheres model, of the order  $10^7$  at 400 nm, is lower than for the surface protrusion model but several orders of magnitude higher than for a single isolated 45 nm sphere.

From the data in Fig. 5 and Fig. 6 it is clear that one needs to construct shapes that differ substantially from the spherical symmetry in order to obtain EM-enhancement factors of the same order as those found for the dimer case. On the other hand, it is clear that the presence of sharp protrusions

or crevices together with RR effects could, in principle, lead to enhancement effects for single particles similar to those reported in the recent single-molecule SERS experiments. The question is whether these types of structures are realistic. Judging from the highly irregular particle shapes evident in Fig. 1, this possibility cannot be ruled out. However, to our knowledge, no experimental data that conclusively links "hot sites" to surface protrusions or crevices has been presented so far. High resolution imaging of "hot" single particles could resolve this issue, and serve as a critical test of electromagnetic SERS theory.

#### IV. CONCLUSIONS

We have reported and analyzed calculations of electromagnetic enhancement effects of relevance to single-molecule surface enhanced Raman scattering (SERS). Data for single and paired spherical and nanocrystal shaped particles composed of Ag or Au are presented, and the effects of surface protrusions are investigated. We find a large and spatially confined electromagnetic enhancement effect, of the order  $10^{11}$ , only for the case of strongly coupled structures, such as dimer configurations or sharp protrusions. In these cases, electromagnetics is likely to produce the dominant contribution to single molecule sensitivity in SERS. However, an additional "chemical" SERS effect has to be invoked in order to bridge the gap to the highest SERS enhancement factors, of the order  $10^{14}$ , reported in the literature. Single spherical or nanocrystal shaped particles are found to produce a comparatively weak electromagnetic enhancement effect, indicating their inefficiency as substrates for single molecule SERS. The calculated optical response of the investigated structures is highly dependent on wavelength and polarization. Thus, single molecule SERS coupled with high resolution imaging can be used as an efficient experimental test of the electromagnetic theory of surface enhanced Raman scattering.

#### ACKNOWLEDGMENTS

M.K. and P.A. gratefully acknowledge financial support from the Swedish Foundation for Strategic Research and the Swedish Natural Science Research Council, respectively.

- 
- [1] For a review see M. Moskovits, Rev. Mod. Phys. **57**, 783 (1985).
  - [2] K. Kneipp *et al.*, Phys. Rev. Lett. **76**, 2444 (1996).
  - [3] S. Nie and S.R. Emory, Science **275**, 1102 (1997).
  - [4] K. Kneipp *et al.*, Phys. Rev. Lett. **78**, 1667 (1997).
  - [5] K. Kneipp *et al.*, Phys. Rev. E **57**, 6281 (1998).
  - [6] H. Xu, E.J. Bjerneld, M. Käll, and L. Börjesson, Phys. Rev. Lett. **83**, 4357 (1999).
  - [7] J.T. Krug II, G.D. Wang, S.R. Emory, and S. Nie, J. Am. Chem. Soc. **121**, 9208 (1999).
  - [8] A. Otto, *Light Scattering in Solids IV*, Topics in Applied Physics Vol. 54 (Springer-Verlag, Berlin, 1984).
  - [9] A. Campion and P. Kambhampati, Chem. Soc. Rev. **27**, 241 (1998).
  - [10] S.R. Emory, W.E. Haskins, and S. Nie, J. Am. Chem. Soc. **120**, 8009 (1998).
  - [11] A.M. Michaels, M. Nirmal, and L.E. Brus, J. Am. Chem. Soc. **121**, 9932 (1999).
  - [12] C.D. Keating, K.M. Kovaleski, and M.J. Natan, J. Chem. Phys. B **102**, 9404 (1998); **102**, 9414 (1998).
  - [13] M. Inoue and K. Ohtaka, J. Phys. Soc. Jpn. **52**, 3853 (1989).
  - [14] J.D. Jackson: *Classical Electrodynamics*, 3rd ed. (Wiley, New York, 1998).
  - [15] J.H. Bruning and Y.T. Lo, IEEE Trans. Antennas Propag. **19**, 378 (1971).
  - [16] S. Stein, Q. Appl. Math. **19**, 15 (1961).
  - [17] O.R. Cruzan, Q. Appl. Math. **20**, 33 (1962).
  - [18] C. A. Brebbia, J. C. Telles, and L. C. Wrobel, *Boundary Ele-*

- ment Techniques (Springer, Berlin, 1984).
- [19] F.J. García de Abajo and J. Aizpurua, Phys. Rev. B **56**, 15 873 (1997).
  - [20] M. Schmeits and L. Damby, Phys. Rev. B **44**, 12 706 (1991).
  - [21] N. Zabala, A. Rivacoba, and P.M. Echenique, Phys. Rev. B **56**, 7623 (1997).
  - [22] P.B. Johnson and R.W. Christy, Phys. Rev. B **6**, 4370 (1972).
  - [23] J.I. Gersten and A. Nitzan, Surf. Sci. **158**, 165 (1985).
  - [24] F.J. García-Vidal and J.B. Pendry, Phys. Rev. Lett. **77**, 1163 (1996).
  - [25] G. Mie, Ann. Phys. (Leipzig) **25**, 377 (1908).
  - [26] R. Ruppin, *Electromagnetic Surface Modes*, edited by A.D. Boardman (Wiley, New York, 1982), p. 349.
  - [27] A. Zangwill and P. Soven, J. Vac. Sci. Technol. **17**, 159 (1980).
  - [28] L.C. Davis, Phys. Rev. B **14**, 5523 (1976).
  - [29] D.S. Wang and M. Kerker, Phys. Rev. B **24**, 1777 (1981).
  - [30] J.I. Gersten, J. Chem. Phys. **72**, 5779 (1980); J.I. Gersten and A. Nitzan, *ibid.* **73**, 3023 (1980).